Mine Water Environ (2016) 35:469–479
DOI 10.1007/s10230-016-0383-7

TECHNICAL ARTICLE

The Relationship Between Flow Paths and Water Quality in Mine Water Oxidation Ponds in South Korea

Dong-Kil Lee[1] · **Young-Wook Cheong**[1]

Received: 19 May 2015 / Accepted: 20 January 2016 / Published online: 19 February 2016

Abstract Tests were carried out at passive mine water treatment sites in South Korea to determine how flow and pH affected other water quality parameters. Computational flow analysis and tracer tests revealed that the water took surprisingly direct flow routes in the oxidation ponds, while other areas remained stagnant. Furthermore, ferrous iron concentration, dissolved oxygen, pH, electrical conductivity, total dissolved solids, turbidity, and water depth were all directly affected by the flow patterns due to the relationship between retention time and iron precipitation.

Keywords Acid · Flow characteristics · Physicochemical property · Whangji-Yoochang · Seokbong

Introduction

Passive treatment oxidation ponds are designed to hold acid mine drainage (AMD) for a certain time period so that the Fe^{2+} contained in the AMD can react with dissolved oxygen (DO) or oxygen in the air so that the iron can precipitate as a ferric hydroxide. Engineering design guidelines for oxidation ponds by the National Coal Board (Banks 2003) recommend that oxidation ponds have a capacity of 1 L/s per 100 m^2 of pond area and a nominal retention time of 48 h (Laine and Jarvis 2003). However, the Fe^{2+} oxidation reaction rate depends on the pH, and thus the retention time of AMD in oxidation ponds should be determined according to the pH of the AMD. Even though the biotic and abiotic iron-oxidizing reactions are complicated (Morgan and Lahav 2007), at a pH of 3 or below, the abiotic oxidation rate of Fe^{2+} in AMD is low and remains relatively constant. On the other hand, when the pH is above 4 (and below 8), the abiotic iron oxidation rate increases exponentially with pH (Kleinmann 2006).

In this follow-on study from Lee et al. (2013), the flow patterns, retention times, and water quality of AMD were evaluated in oxidation ponds at two passive treatment sites (Fig. 1). Given that the oxidative precipitation of Fe^{2+} depends on pH, two oxidation ponds were chosen: the Whangji-Yoochang (WJ) oxidation pond in Samcheok City, Gangwon Province, South Korea (where the pH of the AMD was 6.79) and the Seokbong (SB) oxidation pond in Mungkyeong City, Gyeongbuk Province, South Korea (where the pH was 3.18). In addition, the Samma-Taejeong (ST) oxidation pond in Samcheok City, Gangwon Province, South Korea (where the pH was 2.86) was selected for a turbidity comparison.

In the WJ and ST passive treatment facilities, the AMD drains directly from the mine into the oxidation pond through a 100 m long pipe. After retention, it flows into a successive alkalinity producing system (SAPS) and a constructed wetland. At the SB passive treatment facility, due to the low pH of the AMD, the SAPS is located ahead of the oxidation pond and the wetland is placed after the oxidation pond.

The flow rates of the AMD of the WJ and SB ponds were 59.3 and 86.4 m^3/h, respectively. The Fe^{2+}

Electronic supplementary material The online version of this article (doi:10.1007/s10230-016-0383-7) contains supplementary material, which is available to authorized users.

✉ Dong-Kil Lee
ldk@kigam.re.kr

[1] Korea Institute Geoscience and Mineral Resources (KIGAM), 124 Gwahang-no, Yuseong-gu, Daejeon 305-325, South Korea

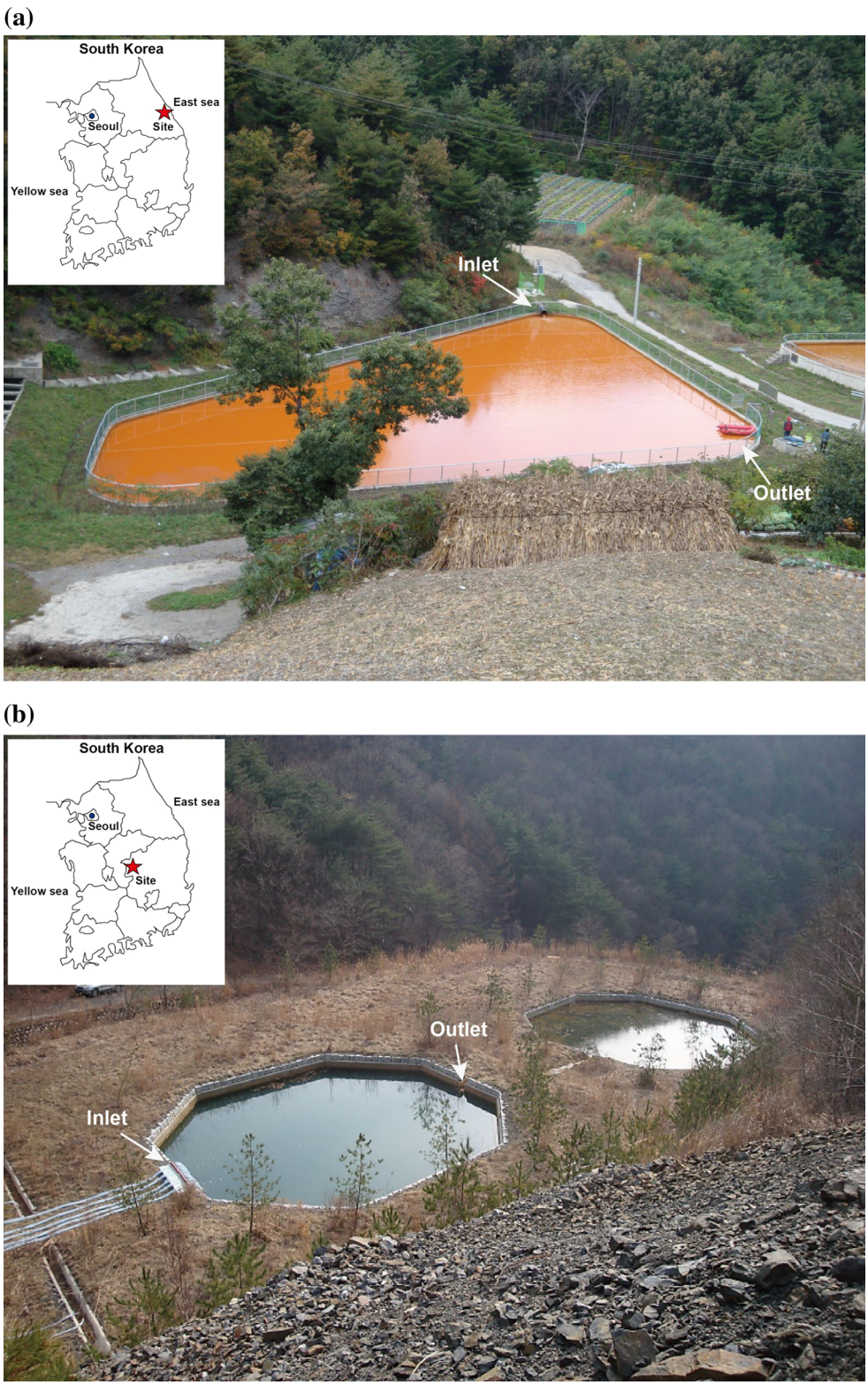

Fig. 1 View of test sites. **a** View of WJ pond. **b** View of Seokbong pond

concentration ($[Fe^{2+}]$) of the AMD was 78 mg/L for the SB pond, but 25.5 mg/L for the WJ pond, while their total Fe content were similar at 136 and 132.5 mg/L, respectively. The ST pond had an $[Fe^{2+}]$ of 81.5 mg/L. This allowed us to study how the flow patterns and water quality of the AMD in the oxidation ponds were related.

Test Methodology

Determination of Measuring Factors

The pH, DO, and temperature were measured using a TOA HM-20P. The EC, TDS, and salinity were measured using an ORION 125A+ conductivity meter. Turbidity was measured using a HACH 2100P turbidimeter. The [Fe^{2+}] was measured in the field using the 1, 10 phenanthroline method (with a HACH DR/2800 colorimeter). In addition, a low specific gravity device with a large contact area was used to measure water depth to the sediment to avoid disturbing the iron hydroxide at the bottom.

Water Tank Test

To identify how the AMD changed with retention time, water quality was monitored in 30 L water tanks, initially at 2 h intervals, and then at longer intervals as variations diminished over time. The National Coal Board (1982) recommends a nominal retention time of at least 48 h. Rather than having to constantly monitor a single tank of AMD for 48 h, two separate water tanks were used into which the AMD was placed 12 h apart. The idea was that by monitoring the two tanks for 12 h for two days, the test could generate 48 h of data. Samples were collected for turbidity and Fe^{2+} measurements over the entire water depth in the tank, whereas samples for the other parameters were collected 10 cm below the water surface.

In-Situ Distribution Tests

In determining the measuring and sampling points, which will be referred to measuring points hereafter, the pond was divided into a grid (Fig. 2). There were 30 measuring points in the WJ pond and 23 in the SB pond. A liquid layer sampler was used to obtain vertical column samples for measuring [Fe^{2+}] and turbidity. Care was taken not to disturb the AMD while moving from one point to the other by boat. Measurements were made 0.3 m below the water surface.

Tracer (Dye) Test

To visualize the flow pattern of the AMD in the pond and to evaluate the flow characteristics, an edible dye (Blue #2) was injected as a tracer. The dye was diluted to 168 ppm and injected at the inlet; the inflow age was measured by checking the time required for the dye to reach the preset measuring points of the grid.

Computational Flow Analysis

The air age concept (used in air conditioning systems) was applied to calculate the retention time of the AMD in the oxidation ponds. Flow analysis was carried out using three governing equations of continuity, movement, and the $k - \varepsilon$ turbulent-dissipation equation. FLUENT, a computational fluid dynamics (CFD) program that uses the finite volume method was used as the analysis software. The 2^{nd} order upwind scheme was used for discretization. The AMD flowed into the pond at a constant flow rate and was discharged to the outlet at atmospheric pressure. Therefore, the inlet was assigned as a boundary condition of constant flow rate and the outlet was assigned the condition of constant pressure. A user-defined scalar was used to calculate and identify the inflow age distribution.

Results and Discussion

Initial values of some measuring factors were significantly different for each pond because the sampling and measuring times differed; note that in this study, actual data, instead of normalized data, was used to represent the site conditions accurately. It should also be noted that the AMD properties changed over time. The trend line in the water tank test results indicates the trend of measurements, and is not a mathematical fitting. The in situ distribution test result was generated by interpolation by ordinary kriging, using Surfer software (Golden Software Inc.).

Flow Pattern and Retention Time of the Whangji-Yoochang Oxidation Pond

Figure 3 shows the computational flow analysis of the WJ pond. Streamlines in Fig. 3b describe a family of curves that are instantaneously tangent to the velocity vector of the flow and show the direction a massless fluid element will travel at any point in time (NASA 2015). The governing flow by which the AMD flowed from the inlet to the outlet is along the bottom of the trapezoidal shape of the pond; the rest of the flow is divided by eddies, making it difficult for that AMD to flow towards the outlet. The velocity on the surface of the pond is depicted in Fig. 3a; a high velocity was detected along the bottom wall from the inlet to the outlet, while a very low velocity was observed in the rest of the pond. The distribution of the inflow age can be seen in Fig. 3c; a lower inflow age was observed along the pond's bottom wall, while older water occurred in the upper area where the flow was relatively stagnant.

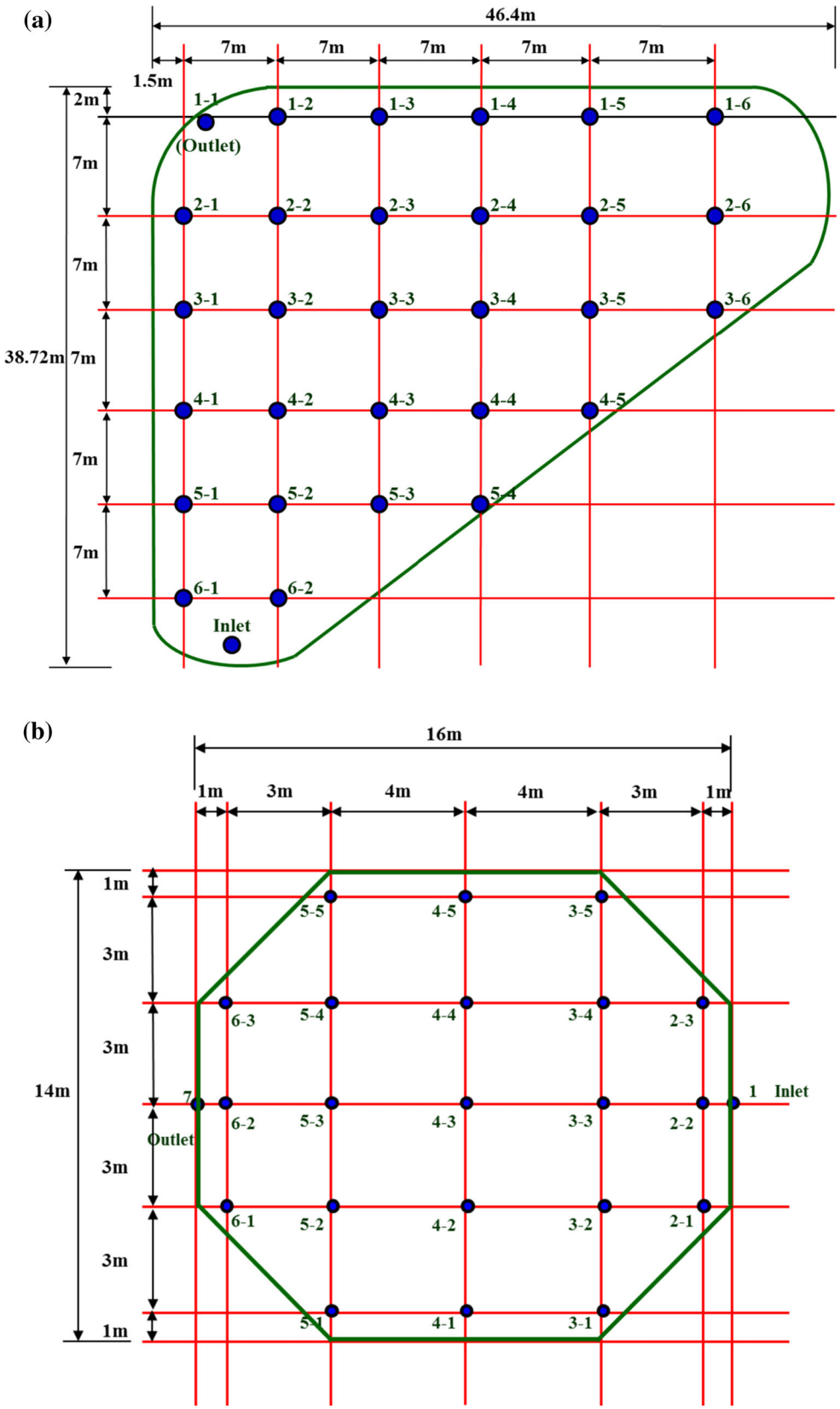

Fig. 2 Measuring points of ponds. **a** Measuring points of WJ pond. **b** Measuring points of SB pond

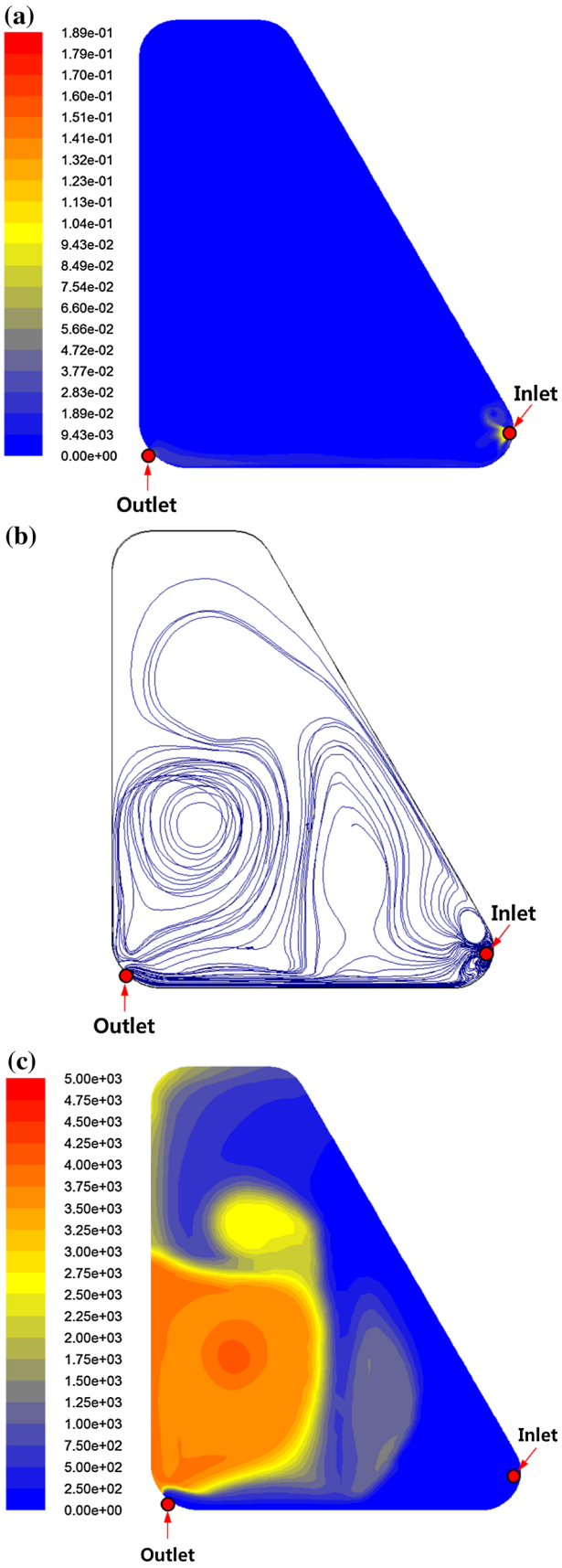

◀**Fig. 3** Flow characteristics by computational flow analysis in WJ pond. **a** Distribution of velocity (m/s). **b** Distribution of streamline. **c** Distribution of inflow age (min)

The tracer test dye mostly spread along the pond bottom, flowing between the inlet and the outlet in 40 min, and gradually extended to the right side at 80 and 140 min (Fig. 4). The blue dashed line depicts the predicted dye distribution; the spread of the dye in the field and its retention time correlated relatively well with the CFD results.

Flow Pattern and Retention Time of the Seokbong Oxidation Pond

Figure 5 shows the computational analysis for the SB pond. The velocity distribution between the inlet and outlet is illustrated in Fig. 5a. The cross-sectional velocity distribution map shows that the AMD moved at a relatively high velocity to the floor of the pond near the outlet, but that prior to that, the high velocity flow was mostly on the pond surface. The streamline consists of a main flow that links the inlet to the outlet, and stagnant areas that formed on either side of the main flow (Fig. 5b). As indicated in Fig. 5c, a low inflow age formed along the line linking the inlet and outlet and a high inflow age formed in the surrounding areas, which was considered to be stagnant. The distribution of inflow age on the cross section of the pond showed that an area of low inflow age formed near the surface and extended to the floor of the pond as the AMD flowed towards the outlet. Thus, most of the flow was moving from the inlet to the outlet along the surface of the pond, failing to reach deeper levels.

The injected dye flowed along the main flow, while the dye on either side of the main flow was stagnant—though the dye eventually spread out due to concentration differences (Fig. 6). It only took about 2 min for the dye to flow from the injection point to the outlet. As the test was conducted in the field with various unexpected factors, the results from the experiment and the results from the computational analysis did not exactly coincide.

Variation of Ferrous Concentration

The $[Fe^{2+}]$ of the WJ pond fell exponentially over time (Supplemental Fig. 1a), similar to what was observed by Hedin (2008). The $[Fe^{2+}]$ of the SB pond rapidly decreased for the initial 6 h and then remained relatively constant until 30 h had passed, at which time the $[Fe^{2+}]$ started to decrease gradually (Supplemental Fig. 1b). Given that AMD with a low pH has a much slower Fe^{2+} reaction rate than at a circumneutral pH, it is clear that retention time in

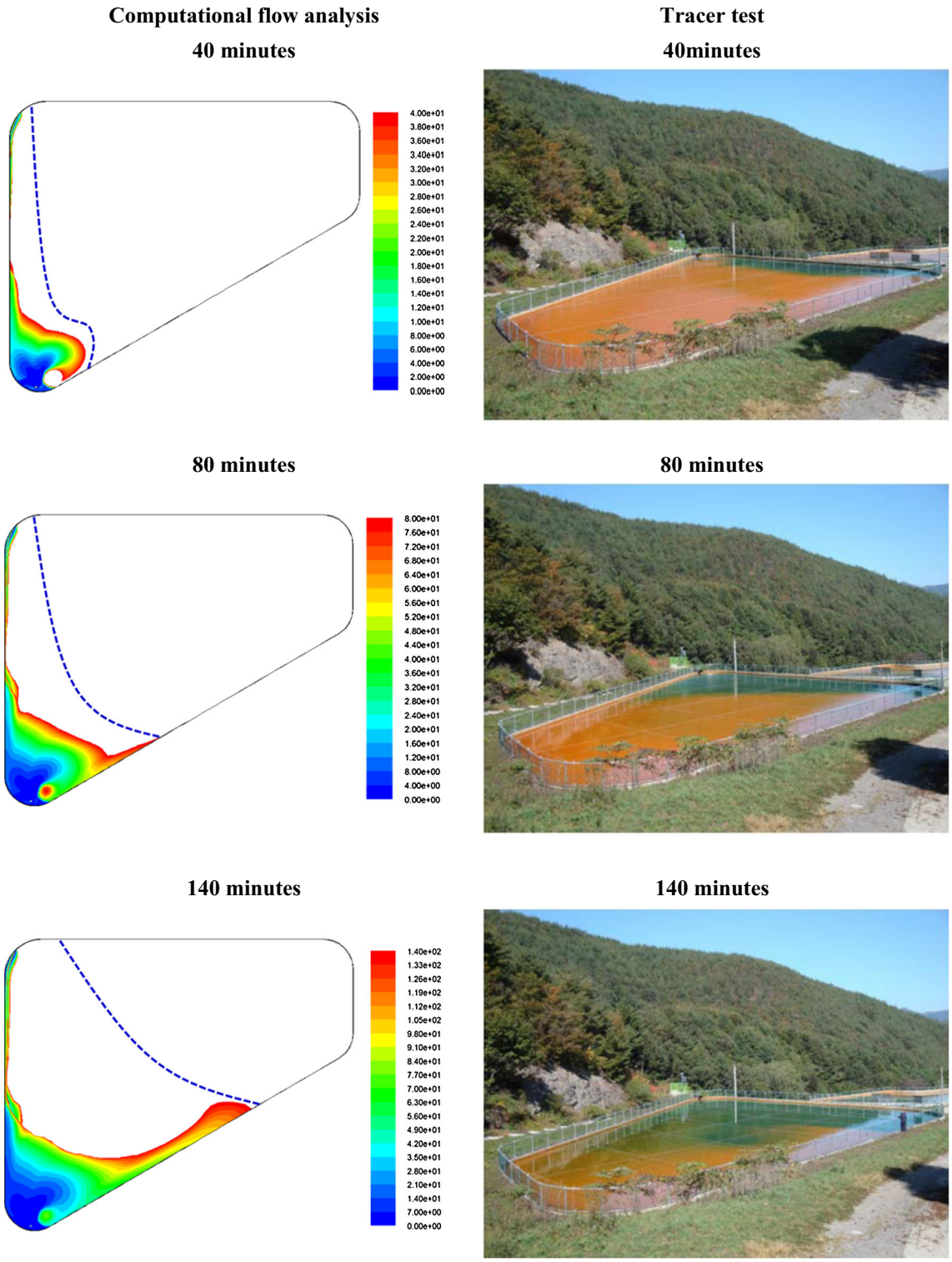

Fig. 4 Dye spread in WJ oxidation pond

the low pH pond should be extended. The [Fe^{2+}] in the WJ pond was high around the inlet area and decreased rapidly to about 10 mg/L as the AMD spread out (Supplemental Fig. 2a).

This tendency can also be seen in Supplemental Fig. 2b, where except for the lower value shown in the left side of the pond, the [Fe^{2+}] in the SB pond was around 70 mg/L, which is much greater than in the WJ pond. This is

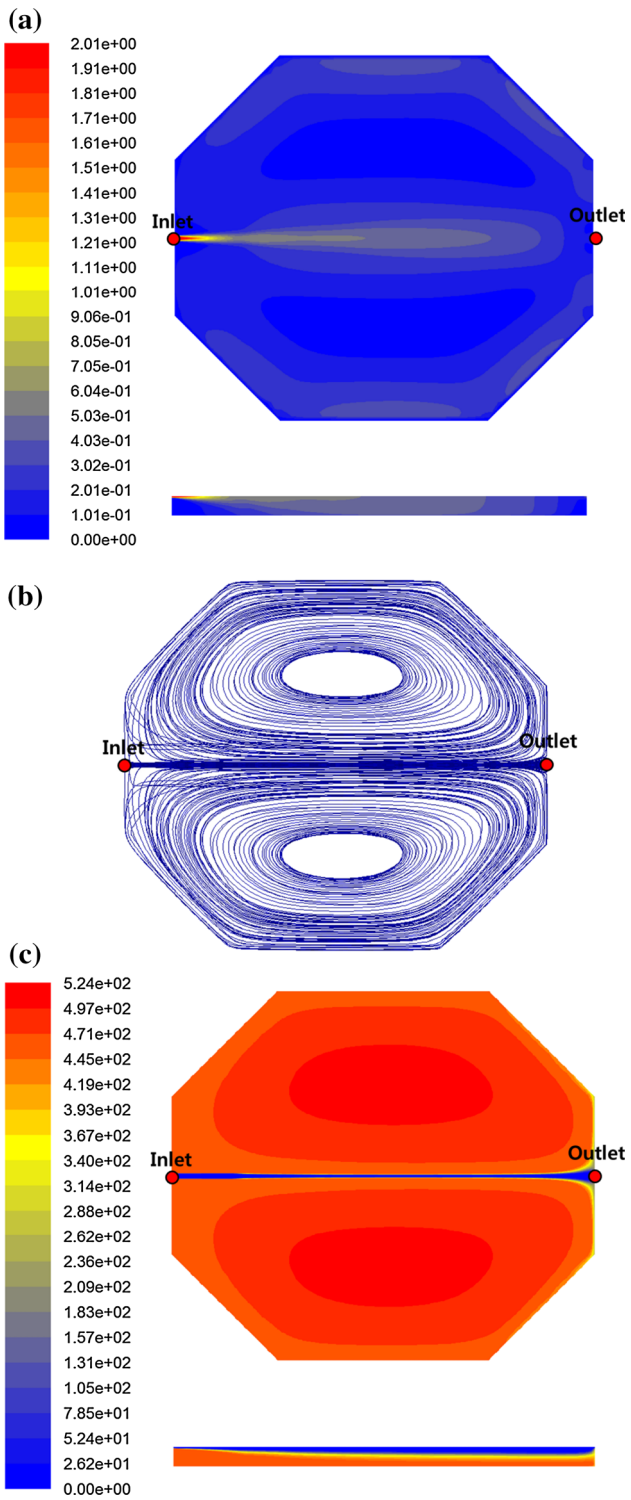

Fig. 5 Flow characteristics by computational flow analysis in SB pond. **a** Velocity (m/s) (plan, section). **b** Streamline (plan). **c** Inflow age (min) (plan, section)

attributed to the insufficient retention time provided for Fe^{2+} oxidation in the SB pond, given its pH. The time required for iron precipitation generally decreases as the pH gets closer to neutral. The Fe^{2+} removal rate in the WJ pond reached 95.6 % after 60 h, while it only reached 13.5 % in the SB pond for the same time duration. The Fe^{2+} was rapidly removed initially in the WJ pond, but more slowly in the SB pond.

Dissolved Oxygen (DO)

As indicated in Supplemental Fig. 1c, DO decreased for the first 6 h after the AMD was put into the WJ tank; this is attributed to the fast oxidation process. After that, the oxygen supplied through the water surface and the oxygen consumed by Fe^{2+} oxidation reached equilibrium, maintaining the DO at a constant level. However, after 20 h, the oxygen supply started to exceed consumption, causing DO to increase. As shown in Supplemental Fig. 2c, the DO concentration in the WJ pond initially dropped sharply and then gradually decreased as the AMD moved along the main flow. The DO value was relatively high ($\approx$6 mg/L) in the main flow, but gradually decreased to 4.8 mg/L at the bottom (a stagnant area) where retention time was extended. Hence, DO in the WJ pond corresponded well to the inflow age and flow pattern.

The DO in the SB pond gradually decreased for the first 6 h of monitoring and, after that, it was stable, until 27 h has passed, after which the DO again began to decrease (Supplemental Fig. 1d). This variation in the DO concentration was very similar to how [Fe^{2+}] varied. Interestingly, the DO dropped nearly to 0. According to Supplemental Fig. 2d, which shows the DO distribution in the SB pond, the DO was highest near the inlet and decreased as the AMD moved towards the outlet. Also, DO was low on both sides of the stagnant area in a quasi-symmetrical arrangement. Due to the short retention time in this pond, the DO level did not show significant changes.

Electric Conductivity (EC), Total Dissolved Solid (TDS), and Salinity

The tank EC values can be seen in Supplemental Fig. 1e; starting at 1860 µS/cm, the EC dropped to 1800 µS/cm during the first 6 h, and decreased gradually thereafter. Since the EC is related to the total quantity of ions in the water, it was high in the inflow water where the [Fe^{2+}] was relatively high and tended to decrease as the AMD moved through the pond (Supplemental Fig. 2e). However, the EC remained fairly constant on the right side of the pond where the flow was stagnant.

As for the SB pond, the EC variation and distribution are illustrated in Supplemental Figures 1f and 2f, respectively. EC in the SB pond varied only slightly, around 2.6 mS/cm, which then decreased after 40 h. Variation of the EC is attributed to interaction of Fe^{2+} and Fe^{3+}, resolution of

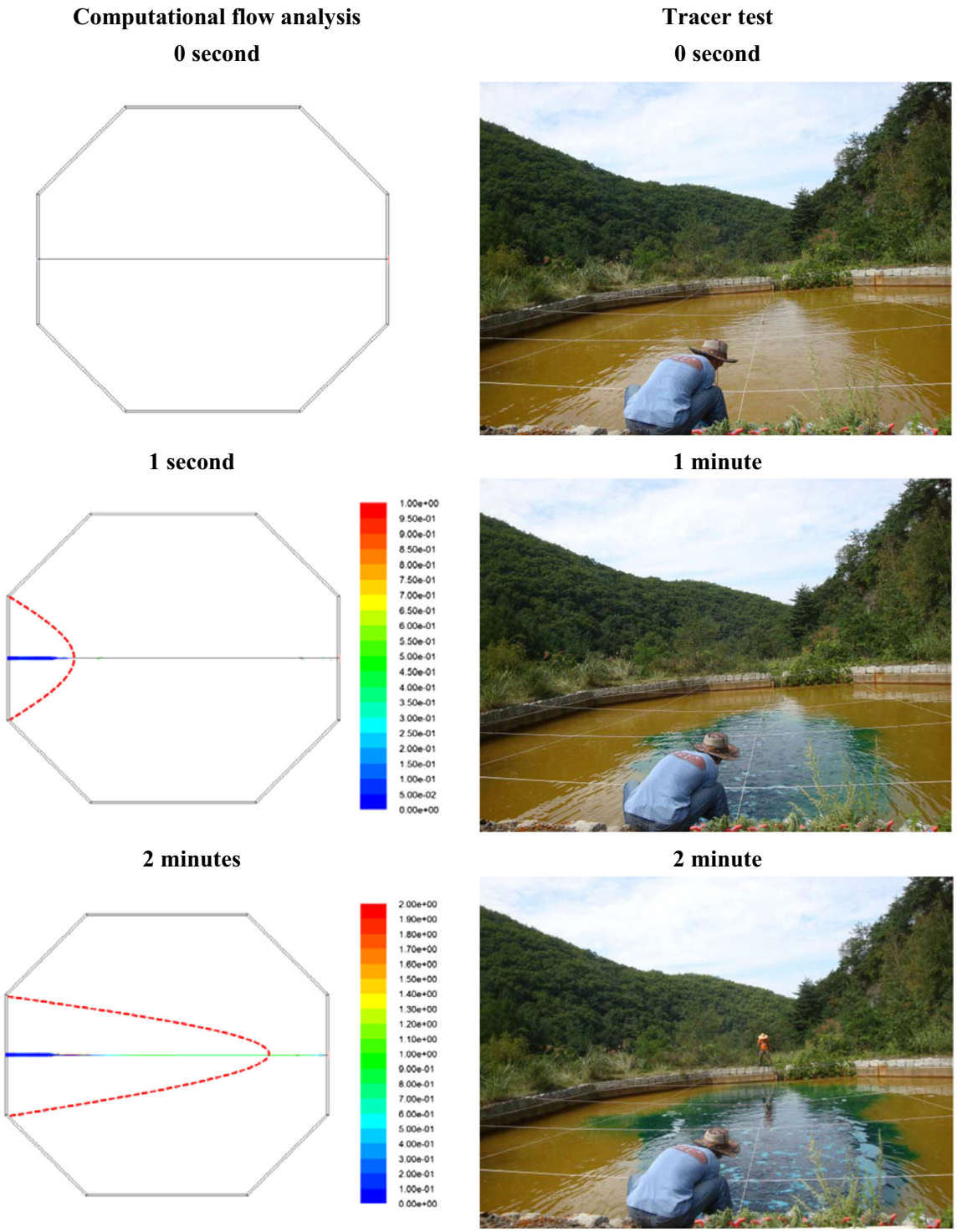

Fig. 6 Spread of the tracer in SB pond

deposits and temperature, etc. (Supplemental Fig. 2f). In general, as the pH moves away from 7, EC tends to increase, which could explain why the AMD in the SB pond might have an initially higher EC value than the WJ pond. TDS and salinity trends are similar to that of EC.

Oxide Reduction Potential (ORP)

ORP measurements were uncertain in the WJ pond and thus were described as a dashed line after 10 h in Supplemental Fig. 1g. The ORP rapidly increased from −2.7

to 46.6 mV over the first 2 h and then remained constant. The AMD, when it initially flowed into the pond, was met with a reduction-dominant environment with an ORP of −2.7 mV; as the environment changed to an oxidation-dominant one through contact with atmosphere, the ORP rapidly increased to 46.5 mV. This tendency is similarly shown in Supplemental Fig. 2g, in that the ORP rapidly increased as the AMD spread out from the inlet. The contour line of the ORP extended with the main flow, while there was little variation on the right side of the pond, where the flow was stagnant.

The ORP started at 401.9 mV (Supplemental Fig. 1h) and increased to 425.6 mV after 4 h, and then remained constant until 40 h had passed, after which it gradually increased again. This was similar to the [Fe^{2+}] pattern of Supplemental Fig. 1b, indicating that the ORP increased because the AMD was exposed to an oxidizing environment. Supplemental Fig. 2h shows the ORP distribution of the Seokbong pond. The ORP value was lowest at the inlet and rapidly increased as the AMD spread out. After a certain distance, it stabilized at 429 mV.

pH

Supplemental Figures 1i and 2i show how the pH tends to decrease over time in the WJ pond as the iron oxidized, hydrolyzed, and precipitated. The should have continued throughout the entire process, but pH increased slightly after 25 h, which is speculated to be due to changes in AMD composition. Supplemental Figures 1j and 2j show that the pH in the SB pond showed similar tendencies, in that the pH decreased as the AMD moved closer to the outlet. An additional increase in pH near the outlet was again attributed to compositional changes in the AMD.

Turbidity

The initial grain size of the hydrated iron formed by Fe^{2+} oxidation is very small (2.5 μm; Younger et al. 2002). Turbidity is influenced by the generation rate of hydrated iron. Turbidity may also increase due to refloating of precipitates by convectional flow caused by temperature differences. Figure 7a, b shows results from when the water tank was coated with an insulation material to minimize thermal transfer between the AMD and the surroundings (Lee et al. 2008). Figure 7a shows turbidity variations in the WJ tank (pH 6.42, [Fe^{2+}] 14.2 mg/L); turbidity was highest during the initial 6 h when oxidation/precipitation reactions were active, and then decreased gradually over time as the precipitates gradually settled. In contrast, turbidity in the ST tank was very low, with a constant value of 1.1 NTU.

Supplemental Figures 1k and 1l show turbidity and temperature in the commercial PVC water tanks, which were sensitive to ambient temperature because of their thin (5 mm or less) composition. Both showed similar tendencies, though with a slight time delay. It was observed that the turbidity resulted from convectional flow caused by the temperature differences between the upper and lower parts of the tanks and the effects of the wide daily temperature range.

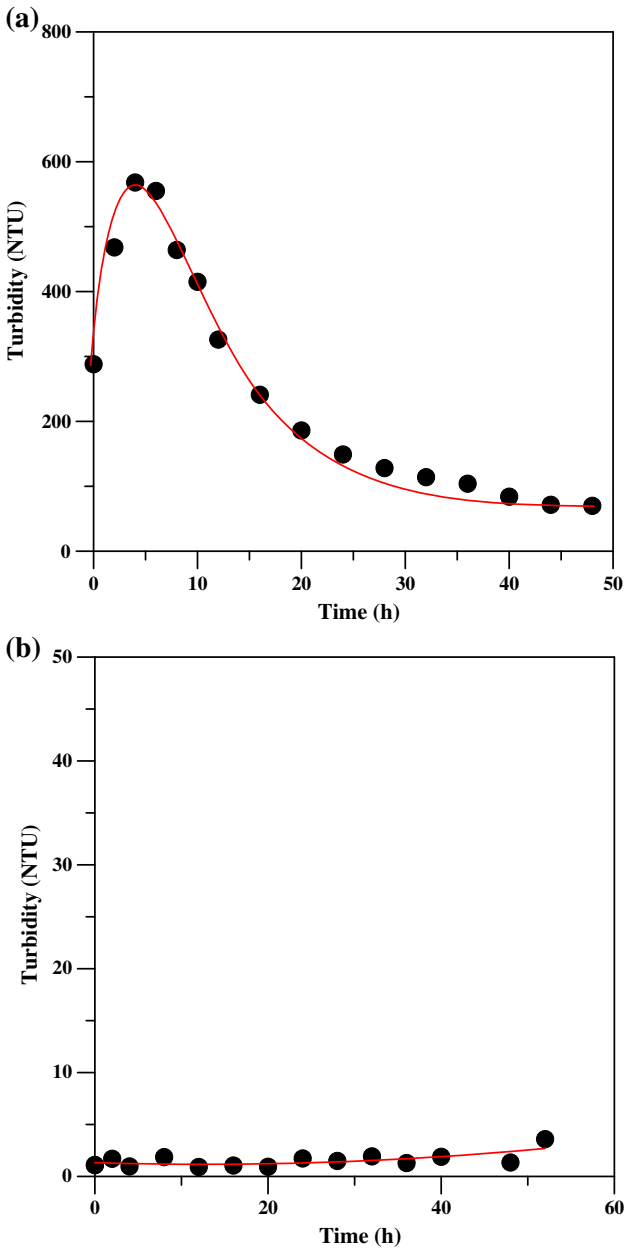

Fig. 7 Variation of turbidity in oxidation ponds (Lee et al. 2008). **a** WJ pond. **b** Samma-Taejeung pond

Supplemental Figure 2k shows the distribution of turbidity in the WJ pond. The turbidity gradient near the inlet was high and declined as the AMD spread away from the inlet because of the difference in Fe^{2+} oxidation rates.

Table 1 Properties of the water at the inlet and outlet of the oxidation ponds

	The Whangji-Yoochang pond			The Seokbong pond		
	Inlet	Outlet	Removal efficiencies (%)	Inlet	Outlet	Removal efficiencies (%)
Fe^{2+} (mg/L)	25.5	7.1	72.2	78	67.5	13.5
DO (mg/L)	8.12	5.78	28.8	7.31	6.63	9.3
pH (−)	6.79	6.7	1.3	3.18	3.18	0.0
EC (μS/cm)	1872	1750	6.5	2.64	2.6	1.5
TDS (mg/L)	942	878	6.8	1343	1323	1.5
ORP (mV)	−66.2	16.4	−124.8	417.3	425.6	−2.0
Temperature (°C)	16.0	19.6	−22.5	18.2	18.4	−1.1
Turbidity (NTU)	134	496	−270.1	243	284	−16.9

There were large variations in turbidity in the stagnant area because the precipitates floated up to the surface due to temperature differences in the pond.

Supplemental Figure 2l shows the turbidity in the SB pond. Unlike the WJ pond, highly turbid conditions did not occur, and turbidity was rather constant at 240–260 NTU; turbidity was higher where the flow was relatively stagnant.

Water Depth

Supplemental Figure 2m shows the distribution of water depth in the WJ pond. As iron precipitation occurs abruptly near the inlet, the precipitates are mostly accumulated there, forming a shallow area. The depth then gradually increases in the rest of the pond. But in the SB pond (Supplemental Figure 2n), iron precipitation occurs very slowly and settle on both sides of the pond. Thus, the area of precipitation deposit depends on the retention time and Fe^{2+} oxidation rate.

Discussion

Table 1 shows the properties of the AMD of each oxidation pond at the inlet and outlet. As indicated, the Fe^{2+} removal efficiency in the WJ pond was as high as 72.2 %, while it was only 13.5 % in the SB pond. The considerable discrepancy in removal efficiency is attributed to the Fe^{2+} oxidation rate, which is affected by pH, and each pond's flow characteristics and retention time.

Dietz (2008) states that the oxidation rate between pH 5 and 8 doubles for every 0.15 pH increase. Generally, when the pH is relatively high, as in the WJ pond, DO tends to decrease quickly because of rapid Fe^{2+} oxidation. The significant decrease in $[Fe^{2+}]$ in turn causes the EC and TDS to decrease. ORP changes from a negative value in a reducing environment to a positive value in an oxidative environment as the AMD flows into the oxidation pond. Due to the initially fast Fe^{2+} oxidation rate, turbidity increases significantly, but then it gradually decreases. Also, iron precipitates along the main flow linking the inlet to the outlet, the DO concentration as well as water depth decreases. On the other hand, in the SB pond, where the pH was close to 3, the DO decrease was smaller due to the slow Fe^{2+} oxidation rate and low variation of EC and TDS. ORP in the SB oxidation pond increased only minutely as the AMD was discharged into the oxidation pond. The increase in turbidity was also small due to slow generation of iron precipitate.

In general, passive treatment systems are most effective for treating typical flow conditions and circumneutral pH water quality (Skousen et al. 1998; Ziemkiewicz et al. 2003), though treatment effectiveness and downstream benefits may diminish as conditions deviate from normal. Cravotta (2010) notes that treatment performance for a wide range of flow conditions is poorly documented in the literature. As our tracer tests and computational flow analyses show, the flow of mine water in an oxidation pond consists of a main flow zone that links the inlet to the outlet, and stagnant zones. Thus, AMD properties that depend on retention time reflect the flow characteristics in the oxidation pond.

Conclusions

In the WJ pond, deposits of precipitates were mostly concentrated near the inlet area due to rapid iron precipitation there, and the amount of deposits decreased as the AMD flowed towards the outlet. In the SB pond, however, iron precipitation occurred very slowly and thus deposits were mostly concentrated along the sides of the pond rather than near the inlet or outlet area.

The Fe^{2+} concentration, DO, pH, EC, TDS, turbidity, and water depth were found to be directly affected by the flow pattern, the iron precipitation reaction rate, and retention time. The Fe^{2+} oxidation rate was dependent on the pH and flow characteristics of the AMD, which in turn were dependent on the retention time in each pond.

Acknowledgments This research was supported by a Research Project of the Korea Institute of Geoscience and Mineral Resources and Mine Reclamation Corporation with funds from the Ministry of Science, Information and Communications Technology, Future Planning of Korea, and the Ministry of Trade, Industry and Energy of Korea.

References

Banks SB (2003) The UK coal authority minewater-treatment scheme programme: performance of operational systems. Water Environ J 17:117–122

Cravotta CA III (2010) Abandoned mine drainage in the Swatara Creek Basin, southern anthracite coalfield, Pennsylvania, USA: 2. performance of treatment systems. Mine Water Environ 29:200–216

Dietz, J (2008) Aeration approaches and activated iron solids (AIS) for AMD treatment. In: Proceedings of PA abandoned mine reclamation and coal mining heritage conference. http://www.treatminewater.com/2008/Presentations.html#141. Accessed 7 July 2015

Hedin RS (2008) Iron removal by a passive system treating alkaline coal mine drainage. Mine Water Environ 27:200–209

Hedin RS, Watzlaf GR, Nairn RW (1994) Passive treatment of acid mine drainage with limestone. J Environ Qual 23:1338–1345

Kleinmann RLP (2006) At-source control of acid mine drainage. https://www.imwa.info/bibliographie/09_14_085-096.pdf

Laine DM, Jarvis AP (2003) Engineering design aspects of passive in situ remediation of mining effluents. Land Contam Reclam 11:113–125

Lee DK, Yim GJ, Cheong YW, Sim YS, Park HS, Jung WH (2008) Variation of ferrous ion contents in mine drainage by oxidation reaction in water tanks. J Korea Soc Geosyst Eng 45:546–557

Lee DK, Yim GJ, Ji SW, Cheong YW (2013) Study on distribution characteristics of some water parameters properties of mine drainage in an oxidation pond, Hwangji-Yuchang coal mine, South Korea. Environ Earth Sci 68:241–249

Morgan B, Lahav O (2007) The effect of pH on the kinetics of spontaneous Fe(II) oxidation by O_2 in aqueous solution-basic principles and a simple heuristic description. Chemosphere 68:2080–2084

NASA (2015) Definition of streamlines. NASA Glenn Research Center Website. http://www.grc.nasa.gov/WWW/k-12/airplane/stream.html. Accessed 7 July 2015

National Coal Board (1982) Technical management of water in the coal mining industry. Mining Dept, London

Singer PC, Stumm W (1970) Acidic mine drainage: the rate-determining step. Science 167:1121–1123

Skousen JG, Rose AW, Geidel G, Foreman J, Evans R, Hellier W (1998) Handbook of technologies for avoidance and remediation of acid mine drainage. National Mine Land Reclamation Ctr, Morgantown

Younger PL (2000) The adoption and adaptation of passive treatment technologies for mine waters in the United Kingdom. Mine Water Environ 19:84–97

Younger PL, Banwart SA, Hedin RS (2002) Mine water: hydrology, pollution, remediation. Springer Science + Business Media, Dordrecht

Ziemkiewicz PF, Skousen JG, Simmons J (2003) Long-term performance of passive acid mine drainage treatment systems. Mine Water Environ 22:118–129